International Journal of Fatigue, Volume 127, October 2019, pp. 275-290
DOI:10.1016/j.ijfatigue.2019.06.017

Accepted manuscript

Notch Effect on Strength and Fatigue Life of Woven Composite Laminates

Ao-Shuang Wan[1], Yi-geng Xu[2], Jun-Jiang Xiong[1]*

1 School of Transportation Science and Engineering, Beihang University, Beijing, 100191, People's Republic of China (*, corresponding author: jjxiong@buaa.edu.cn)

2 School of Aerospace, Transport and Manufacturing, Cranfield University, Cranfield, MK43 0AL, United Kingdom

ABSTRACT This paper presents an experimental and numerical study of the notch effect on strength and fatigue life of double edge notched (DEN) composite laminates made of woven glass fibre lamina 3238A/EW250F and woven carbon fibre lamina 3238A/CF3052. Experimental results show that the notch effect is dependent on fibre type, notch depth, load type and load sequence. A $s-n-R-d-r$ residual strength model was proposed to account for the effects of the notch and the stress ratio, and a progressive damage algorithm was developed to predict damage propagation and residual life of composites under spectrum fatigue load. Good agreement between the experimental results and the numerical predictions has been achieved.

KEYWORDS notch effect; woven composite laminates; fatigue; block loading; life prediction

1. INTRODUCTION

Woven composite laminates are widely used in aerospace, transport and renewable energy industries due to their excellent shear strength, impact resistance and fracture toughness[1]. A main concern is the potentially significant drop to the strength and fatigue life due to the structural discontinuities which are introduced either for functional purposes in the form of notches and cutouts or accidently during manufacture and service in the form of defects. Reliable evaluation of notch effect on structural integrity remains a challenge to the industry, particularly for laminated woven composite components with complex failure mechanisms and interactions. A great deal of research has been conducted to investigate the effect of notches on the mechanical performance of fibre reinforced composite laminates under static and fatigue loads. It has been reported that the strength and fatigue behavior of both the UD-based laminates and woven composite laminates are significantly affected by the notch location (single-edge notch[1], double-edge notches[2] and central hole[3-12]), notch shape (circular hole,

elliptical hole and rectangular slot[3,4]), and notch size[4-7]. Fatigue damage mechanisms of notched composites are different to those of un-notched composites. In contrast to the wide spread of damage initiation sites along the length of un-notched composites, damage usually initiates at the notch and then split occurs and propagates tangent with hole in notched composites[8,9]. The damage growth rate and direction and the failure modes of laminated composite components are also dependent on many factors including fibre type[3], matrix ductility[10], stacking sequence[7,11], and load type[12].

Owing to the complexity in failure mechanisms and their interactions, there is no satisfactory progress in developing a widely accepted micro-level physical damage model to incorporate all the key parameters affecting the fatigue damage process of composite laminates[9,13]. Instead, a lot of cumulative damage models were developed to quantify the fatigue damage development in composites, which include Miner damage models, residual strength models, and residual stiffness models[14]. Miner damage models are simple and practical but do not consider the load sequence effect. Based on experimental results and numerous literature data, Found and Quaresimin[15] reported that the Palmgren-Miner linear damage rule was invalid for some composites including woven composite laminates. Sarfara[16] suggested that both linear and nonlinear Miner rules were inadequate for estimating the accumulated damage of composite joints under block loading. Epaarachch[17] tried four linear and nonlinear Miner models to estimate the damage accumulation of composites under two and three repeated block loading cases but found none of the models performed at reasonable confidence level. Residual strength models can predict the residual strength and the final failure by relating to the applied stress, which is essential for ensuring the capacity of composite structures to carry the design load in the case of extreme overloads appearing in regular cyclic loading[18, 19]. Chen et al[20] combined the residual strength model with frequency domain analysis to predict the fatigue life of woven composite laminates under random spectrum loading and obtained good correlation with experiment results. A major issue with the current residual strength model is the requirement of a large number of specimens to obtain the residual strength data. The advantage of residual stiffness models lies in the fact that stiffness can be measured frequently or even continuously during the fatigue test, whilst residual stiffness models lack the ability to identity the failure modes. Many residual stiffness models[21-23] were demonstrated to be suitable for woven composite laminates by a large number of experiments[24-26]. And a fatigue damage model was developed by combining the crimp model and the shear-lag model to predict the stiffness degradation of woven composite laminates, showing good

agreement between predictions and experimental results[27].

In addition, the residual stiffness and strength models were implemented in the commercial finite element code by Shokrieh and Lessard[28, 29] to assess the fatigue life and progressive damage of composites. Based on the experimental data of UD laminates under longitudinal/transverse tension/compression and in-plane shear fatigue loading, the residual stiffness and strength models are determined and integrated to simulate the degradation caused by fatigue damage. The static failure criteria are modified to identify the fatigue failure of elements. Different failure modes of the ply are detected by the fatigue criteria according to the stress state of each element. Lian and Yao[30] further developed the progressive fatigue damage model by considering the scatter of material properties and proposing a coupled residual stiffness and strength model as damage metric. Eliopoulos et al[31-33] developed a progressive damage simulation algorithm for life prediction of composites with arbitrary lay-up configurations under constant and variable amplitude multi-axial cyclic loading. The above progressive fatigue damage modeling approach is also suitable for woven composite laminates[34]. Two kinds of modeling method based on continuum damage mechanics (CDM) are commonly used in progressive fatigue damage analysis for woven composite laminates. One is to replace the woven fabric with two stacked unidirectional plies corresponding to the warp and weft thicknesses and use the CDM to define the properties of the two virtual unidirectional plies[35]. Another is to establish the meso-scale level (fabric unit cell) models by considering the geometry of yarns[36, 37]. Both of them however need a great number of experiments and mathematical functions, and the meso-scale models need straight inclined segments to depict in more detail the idealized woven fabric geometry including yarn path and cross-sectional shape. The complexity and computational intensity of the modelling process are the main constraint for their application.

It has been observed that most of the research on notch effect have been focusing on the influence of central hole on tensile fatigue behavior of composite laminates. The research of the notch effect on compressive fatigue behavior is very limited, especially for double edge notch effect. Moreover, little quantitative results can be found in literature to characterize the notch effect on fatigue behavior and life prediction of woven composite laminates under spectrum loading. This research aims to fill the gap in the understanding of the effect of double edge notches on the strength and fatigue life of woven composite laminates under various loading condition and notch depth through a detailed experimental and numerical study.

2. MATERIALS AND TEST PROCEDURES

2.1. Materials and specimens

The test specimens were made of woven carbon fibre reinforced polymer 3238A/CF3052 and woven glass fibre reinforced polymer 3238A/EW250F, respectively. Table 1 presents the mechanical properties of the two materials. Both the woven glass fibre and the woven carbon fibre laminate specimens have the same stacking sequence of $[(45/-45)/(0/90)]_{3s}$. Fig. 1 shows the geometry of specimen where 'X' represents the notch depth having the values of 2mm, 3mm, and 4mm for the notched specimens in this study. The laminate plates were fabricated by a vacuum bag process under high temperature of 130 °C and pressure of 0.5MPa. They were cut by a water jet to the size of the specimen. The notches were machined by a steel blade using water cooling.

2.2. Test procedures

All tests were carried out on the hydraulic servo testing machine Instron-8803 at the air moisture in the lab environment. According to ASTM standards D5766-11 and D6484-09[38, 39], all of the specimens were loaded at the rate of 2mm/min until failure during the static tensile and compressive tests. The constant-amplitude and block-loading fatigue tests were performed with the sinusoidal waveform at the loading frequency of 10 Hz. According to ASTM standards D7615-11 and E739-10 [40, 41], the constant-amplitude fatigue tests were conducted under tension-tension (T-T) and compression-compression (C-C) cyclic loading at the stress ratios of 0.05 and 10. For each specimen type, at least four groups of fatigue tests were conducted under different stress levels to achieve four target fatigue lives, namely 10^4, 10^5, 5×10^5 and 10^6 cycles. Each group contained at least three specimens to ensure the reliability of the test data. The specimen which did not fail at the targeted fatigue life under the chosen fatigue stress level was loaded to failure under static load to obtain the residual strength.

Fig. 2 shows the load histories of the high-low (H-L), low-high (L-H), and repeated high-low-high (H-L-H) block-loading fatigue tests. 'S' is the maximum tensile stress when the specimen is subjected to T-T fatigue stress cycles at the stress ratio of 0.05. It is the minimum compressive stress when the specimen is subjected to C-C fatigue stress cycles at the stress ratio of 10. The numbers of the stress cycles in the first loading block in Figs. 2(a-b) are chosen based on the constant-amplitude fatigue experimental results to consume half of the fatigue life of the specimen. The stress spectrum of the H-L-H block loading will be repeated until the failure of the specimen. Similar to the constant-amplitude

fatigue test, at least three specimens were employed for each block-loading fatigue test to ensure the reliability of the test data.

3. EXPERIMENTAL RESULTS AND DISCUSSION

3.1. Notch effect on static and fatigue strength

Table 2 presents the test results of static strengths of un-notched and notched 3238A/EW250F and 3238A/CF3052 specimens. Fig. 3 shows the constant-amplitude fatigue test results of 3238A/EW250F and 3238A/CF3052 composite laminates where N is the fatigue life and S is the maximum absolute value of fatigue stress. The data points labeled with arrows and attendant numbers represent the run-out specimens which did not fail at the targeted fatigue life as mentioned in Section 2.2. The run-out specimens were then loaded up to failure under static load to obtain residual strengths R of these specimens which are plotted in Fig. 4. It is worth pointing out that the lines in Fig. 3 and surfaces in Fig. 4 are the numerical prediction results using the residual strength model developed in Section 4.1. Good agreement between the experimental and numerical results have been achieved.

To assess the effect of the notch depth on static strength reduction and fatigue strength reduction, the strength reduction factor K_T and notch factor K_f are introduced, respectively:

$$K_T = \frac{\sigma_{ud}}{\sigma_{u0}} \tag{1}$$

$$K_f = \frac{S_d}{S_u} \tag{2}$$

where σ_{u0} is the strength of un-notched specimen, σ_{ud} is the residual strength of the notched specimen; S_u is the fatigue strength of un-notched composites at a specified fatigue life (10^6 cycles in this paper), S_d is the fatigue strength of notched composites at the same fatigue life.

Based on the experimental results in Table 2 and Figs. 3 and 4, the strength reduction and notch factor curves were obtained and plotted in Fig. 5. It can be seen from Fig. 5 that both the static and fatigue strength of the notched specimen decreases with the increase of the notch depth, showing the expected detrimental effect of the notch. Moreover, the strength reduction factor curve under tension is below that under compression for both materials, and the notch factor curve under T-T fatigue load is below that under C-C fatigue load, indicating that the notch effect is stronger under tensile static and fatigue load than compressive static and fatigue load.

In addition, the 3238A/CF3052 composite laminates have greater static strength reduction than the

3238A/EW250F composite counterparts but have less fatigue strength reduction than the 3238A/EW250F composite counterparts, showing carbon fibre composites is more sensitive to the notch than glass fibre composites on static strength but is less sensitive to the notch on fatigue strength. This is probably due to the difference between damage mechanisms in the two materials under static and fatigue loads. Actually, the carbon fibre laminate 3238A/CF3052 has more severe stiffness mismatch (or more drastic strain gradient) between the reinforcement and the matrix than the glass fibre laminate 3238A/EW250F as both laminates have the same matrix material. As a result of more severe stiffness mismatch in carbon fibre laminate, the stress concentration around the notch of the carbon fibre laminate is more appreciable than that of the glass fibre laminate, causing greater static strength reduction in 3238A/CF3052 than that in 3238A/EW250F under static loading, and more matrix related damages (such as matrix cracking, fibre matrix debonding, splitting and delamination) in 3238A/CF3052 than in 3238A/EW250F under fatigue loading. It goes without saying that carbon fibre composites is more sensitive to the notch than glass fibre composites on static strength. However, these matrix related fatigue damages in turn redistribute and hence relax the initial high local stress around the notch, and thus the carbon fibre laminate 3238A/CF3052 experiences greater stress relaxation than the glass fibre laminate 3238A/EW250F. It stands to reason that carbon fibre composites is less sensitive to the notch than glass fibre composites on fatigue strength.

3.2. Load sequence effect

Table 3 presents the fatigue test results of the two materials under the block loading. The cumulative damage under block loading is calculated by the Palmgren–Miner linear damage model.

$$D = \sum_{i=1}^{k} \frac{n_i}{N_i} \tag{3}$$

It can be seen from Table 3 that the damage accumulation of woven composite laminates under H-L and L-H block loading do not follow a linear rule. The cumulative damage of 3238A/EW250F laminates under L-H loading is less than 1 but the cumulative damage under H-L loading is greater than 1, which demonstrates a strong load sequence effect on fatigue damage of woven composite laminates and agrees with the findings in literatures[15,16]. Actually, the nonlinearity in fatigue damage accumulation is attributed to the interactions of fatigue damage mechanisms at different stress levels and the stochastic nature of the material properties and loading conditions in real life scenarios[42,43]. Fatigue failure in composite materials occurs as a result of accumulation of various types of micro

damages rather than a dominant crack in metallic materials, which could make the nonlinearity in damage accumulation stronger in composite structures. The fact that L-H load is more damaging than the H-L load for woven composite laminates under tensile fatigue load can be rationalized by the effect of fatigue damages of the first load block on the fatigue damages of the second load block. The large number of low fatigue stress cycles in the first block of the L-H block loading introduces significant matrix related damage leading to multiple delamination and subsequent through-thickness stress and disruption of effective stress transfer between layers. This will cause more fiber breakage and accelerated final failure process in the second block of high fatigue stress in the L-H block loading, making the second block of high stress more damaging than the pure constant high amplitude fatigue loading. As a result, the cumulative damage ratio under L-H block loading is less than 1. On the other hand, the cumulative damage ratio under H-L block loading is greater than 1 as the small number of high stress cycles in the first block better align the fibers in the loading direction, reducing the fraction of the load taking by the matrix in the second block. This will delay the development of the matrix related damages under the low fatigue stress in the second block, making the fatigue stress cycles in the second block of the H-L block loading less damaging than the pure constant low amplitude fatigue loading.

The cumulative damages of woven composite laminates under repeated H-L-H loading are less than 1 for both materials, indicating that frequent transitions and interactions between stress ratios and stress levels significantly shortens the fatigue life of PWF composites. This agrees with findings in literatures[12,16,18] and is associated with the substantial damage that occurs during the transitions between different constant amplitude stress blocks[44]. As shown in Fig.2, the transition between the tensile and compressive stress block during H-L-H loading effectively forms a large stress amplitude loading cycle nearly twice the stress amplitude of the high stress load block. This kind of large transition loading cycle may trigger stronger failure mode interaction and hence can significantly shorten the fatigue life of woven composite laminates due to the brittle nature of the material and the detrimental impact of compressive stress cycle on fatigue life. In addition, the cumulative damage of 3238A/CF3052 laminates is less than that of 3238A/EW250F laminates under repeated H-L-H spectrum load when specimens fail, implying that woven carbon composite laminates are more sensitive to interactions between tensile and compressive loading cycles. This is due to the fact that 3238A/CF3052 laminates have the greater stiffness mismatch between the fibre and the matrix and are

subject to large transition cycles with higher local stress amplitude compared with the 3238A/EW250F laminates.

3.3. Fractographic analysis

To understand the fatigue damage mechanisms of 3238A/EW250F and 3238A/CF3052 laminates, the run-out specimens tested up to the nominal fatigue life of 10^6 cycles were examined under optical microscope. It is found that the damage morphologies of un-notched and double edge notched (DEN) woven composite laminates are similar but the damage morphology under T-T fatigue load is significantly different from that under C-C fatigue load. This is due to the difference in the controlling damage mechanisms under the tensile and compressive fatigue loading conditions. Under tensile fatigue loading, fibre is the main load-carrying element and the fatigue specimens under T-T fatigue loading show fibre-dominated failure modes. In contrast, under compressive fatigue loading, matrix is the main load-carrying element and the fatigue specimens under C-C fatigue loading show matrix-dominated failure modes. Moreover, delaminations are often driven by the shear stress in Mode II under tensile fatigue load, but by the buckling of fibers or plies in Mode I under compressive fatigue load[8].

Under T-T fatigue load, short through-thickness matrix cracks first occur at the edge of specimens (mainly at the edge notches for notched specimens, as shown in Fig. 6, which then propagate into the laminates. The number of matrix cracks increases with the number of loading cycles until a critical crack density is reached. After saturation, they coalesce and further propagate in the forms of debonding and local delamination, Meanwhile, a lot of edge delaminations appear due to the high interlaminar shear stress near the free edges as shown in Fig. 7. The delaminations continue to grow, causing the disruption to the effective stress transfer between fibers and layers. Finally, massive breakage and pull-out of fibers happen as shown in Fig. 8. These are consistent with the findings in literatures[8, 9].

In contrast to the observation under T-T fatigue load, Fig. 9 shows a lot of irregular matrix cracking and delamination instead of short through-thickness matrix cracks under C-C fatigue load. Moreover, local buckling usually happens in compression, accelerating the propagation of delamination during the fatigue process. The composite specimens exhibit mixed shear and interlaminar failure modes in the final stage under C-C fatigue load as shown in Fig. 10, which are commonly observed in woven textile composites under compression [45, 46]. Figs. 10a and 10c show the mixed through-thickness shear

and interlaminar failure modes, where damages propagate at an angle to the loading direction across the thickness of the specimen. Figs. 10b and 10d show the mixed wedge splitting and interlaminar failure mode, where one fractured part of specimen is pushed into the other when final failure happens. Two cracks propagate in the thickness direction to form the wedge and a large delamination happens in the middle with multiple delaminations clearly visible in the failed parts. The two kinds of mixed shear and interlaminar failure mode of specimens under C-C fatigue load happen randomly. In woven composite specimens, the shear planes are usually promoted by the stress concentration due to fibre waviness. The buckling and delamination under compression propagate in one shear plane or two shear planes to converge, forming the two kinds of fracture morphology.

From Figs. 7-10, the difference between fatigue damage of 3238A/EW250F and 3238A/CF3052 composite laminates can be summarized as follows. (i) The fatigue damages (including matrix cracking, debonding and delamination) in 3238A/CF3052 laminates are more widespread than those in 3238A/EW250F laminates (see Figs. 7 and 9). These are consistent with the findings in literature[47]. Particularly in un-notched 3238A/CF3052 laminates under T-T fatigue load, the local and edge delaminations accelerate and expand all over the specimen until the final rupture (shown in Fig. 8c). The reason for the different fatigue damages between the two laminates are the higher applied stress level on 3238A/CF3052 composite laminates and the greater mismatch of stiffness between the fibre and the matrix material in 3238A/CF3052 composites. In reality, to achieve the same nominal fatigue life as that of 3238A/EW250F composites necessitates the higher applied stress level on 3238A/CF3052 composite laminates, causing more matrix cracking and subsequent delaminations in 3238A/CF3052 composites. Meanwhile, the greater mismatch of stiffness between the fibre and the matrix material in 3238A/CF3052 composites always results in greater stress concentration at the fibre-matrix and interlayer interfaces in 3238A/CF3052 in relation to 3238A/EW250F[47], leading to more fibre-matrix debonding and interlayer delaminations in woven carbon composites. As shown in Figs. 8 and 10, the aforementioned widespread damages induce more pull-out of fibers at tensile fatigue failure but more crushing under compressive fatigue loading in 3238A/CF3052 composites compared with 3238A/EW250F composites. (ii) For 3238A/EW250F composites, more damage mechanisms are activated in notched specimens than in un-notched specimens (shown in Figs. 7(a-c) and 9(a-c)) as a result of the high stress level in the notch area. However, for 3238A/CF3052 composites, the fatigue damages in un-notched specimens are more widespread than in notched specimens (shown in Figs.

7(d-f) and 9(d-f), especially for delaminations under T-T fatigue load. As discussed earlier, the delaminations occur more easily in 3238A/CF3052 laminates than 3238A/EW250F laminates due to the greater mismatch in material properties and higher applied stress level in carbon 3238A/CF3052 laminate. In contrast with the notched 3238A/CF3052 specimens, the stress distribution is uniform in un-notched specimens and is high enough to trigger multiple small delaminations along the longitudinal direction. These widespread local delaminations will coalesce to form large delaminations in un-notched 3238A/CF3052 specimens.

4. NUMERICAL PREDICTIONS AND DISCUSSION

4.1. Residual strength model considering the effect of notch depth and stress ratio

Fatigue is the progressive degradation of material properties under repeated cyclic loading. It is hence reasonable to use residual strength to quantify the fatigue damage of the component. Based on Authors' previous work[48], following relation is proposed to correlate the residual strength and the number of fatigue cycles at a given stress ratio of r_0 :

$$n = C\left(s - S_0\right)^p \left[R_0 - R\left(n\right)\right]^q \tag{4}$$

where n is the number of fatigue loading cycles; s is the maximum absolute value of fatigue stress; $R(n)$ is the residual strength after n number of cycles; S_0 is the fatigue endurance limit of composites; R_0 is the initial residual strength of composites obtained by static test; C, p and q are model parameters.

It is also expected that the notch depth has significant influence on the initial residual strength R_0 and fatigue limit S_0. Following relations are assumed among R_0, S_0 and the notch depth:

$$R_0 = R_0^0\left(1 - \alpha_1 d^{\beta_1}\right) \tag{5}$$

$$S_0 = S_0^0\left(1 - \alpha_2 d^{\beta_2}\right) \tag{6}$$

where d is the notch depth; α_1, β_1, α_2 and β_2 are the model constants to be determined; R_0^0 is the initial strength of un-notched composites; S_0^0 is the fatigue endurance limit of un-notched composites.

Substituting Eqs. (5) and (6) into Eq. (4) gives

$$n = C\left[s - S_0^0\left(1-\alpha_2 d^{\beta_2}\right)\right]^p \left[R_0^0\left(1-\alpha_1 d^{\beta_1}\right) - R(n)\right]^q \tag{7}$$

Eq. (7) is the governing equation of the $s-n-R-d$ fatigue residual strength model at a given stress ratio of r_0. The initial residual strength of the notched composite component is usually obtained from the static test, and the model constants α_1, β_1 and R_0^0 are obtained from the static test data by means of the linear regression principle (see Appendix A). Then using the fatigue test results, the model parameters α_2, β_2, S_0^0, p, q and C are determined by best fitting method (see Appendix B). Real engineering structures are rarely under constant-amplitude loading so it is important to account for the effect of stress ratio in the residual strength model. The empirical Goodman diagram[49] shown in Fig. 11 is adopted in this study to modify the $s-n-R-d$ model. Note that the crack growth in homogeneous metal materials primarily occurs in tension as crack tends to close under compressive loads. As a result, the Goodman model for metallic materials does not consider the fatigue damage under compression. For composite materials, crack growth can however occur under compression and should be accounted for. Therefore, following piecewise linear function based on the Goodman model is used to cover all fatigue loading type including compression-compression:

$$\begin{cases} \dfrac{S_a}{S_{-1}} + \dfrac{S_m}{\sigma_t} = 1 & -1 \le r \le 1 \\ \dfrac{S_a}{S_{-1}} + \dfrac{S_m}{\sigma_c} = 1 & r < -1 \text{ or } r > 1 \end{cases} \tag{8}$$

where S_a and S_m are the stress amplitude and mean stress; S_{-1} is the fatigue endurance limit under fully reversed cyclic loading; σ_t is the ultimate tensile strength of the material; σ_c is the ultimate compressive strength of the material; r is the stress ratio.

From the definition of stress ratio r, it can be shown that

$$\begin{cases} S_a = \dfrac{1-r}{2} S_{\max,r} = \dfrac{1-r}{2r} S_{\min,r} \\ S_m = \dfrac{1+r}{2} S_{\max,r} = \dfrac{1+r}{2r} S_{\min,r} \end{cases} \tag{9}$$

where $S_{\max,r}$ is the maximum nominal stress at the stress ratio of r, and $S_{\min,r}$ is the minimum nominal stress at the stress ratio of r.

Substituting Eq. (9) into Eq. (8), the constant life diagram for arbitrary stress ratio r is obtained as

$$\begin{cases} \dfrac{(1-r)S_{\max,r}}{2S_{-1}}+\dfrac{(1+r)S_{\max,r}}{2\sigma_t}=1, & \left(-1\le r\le 1\right) \\ \dfrac{(1-r)S_{\min,r}}{2rS_{-1}}+\dfrac{(1+r)S_{\min,r}}{2r\sigma_c}=1, & \left(r<-1 \text{ or } r>1\right) \end{cases} \tag{10}$$

When r equals the specific stress ratio r_0, Eq. (10) becomes

$$\begin{cases} \dfrac{(1-r_0)S_{\max,r_0}}{2S_{-1}}+\dfrac{(1+r_0)S_{\max,r_0}}{2\sigma_t}=1, & \left(-1\le r_0\le 1\right) \\ \dfrac{(1-r_0)S_{\min,r_0}}{2r_0S_{-1}}+\dfrac{(1+r_0)S_{\min,r_0}}{2r_0\sigma_c}=1, & \left(r_0<-1 \text{ or } r_0>1\right) \end{cases} \tag{11}$$

In order to simplify the formulation of model, the initial strength R_0 is introduced to represent the absolute value of ultimate strength, namely,

$$\begin{cases} R_0=\sigma_t, & \left(-1\le r\le 1,\ -1\le r_0\le 1\right) \\ R_0=-\sigma_c, & \left(r<-1 \text{ or } r>1,\ r_0<-1 \text{ or } r_0>1\right) \end{cases} \tag{12}$$

Note that σ_t and σ_c respectively represent the ultimate strengths on tension- and compression-dominated sections of material and are different values.

Substituting Eq. (12) into Eqs. (10) and (11), and taking transformation of Eqs. (10) and (11) to eliminate S_{-1} yields

$$\begin{cases} S_{\max,r_0}=\dfrac{2R_0(1-r)}{(1-r_0)\left[2R_0-(1+r)S_{\max,r}\right]+(1+r_0)(1-r)S_{\max,r}}S_{\max,r}, & \left(-1\le r\le 1,\ -1\le r_0\le 1\right) \\ \left|S_{\min,r_0}\right|=\dfrac{-2R_0r_0(1-r)}{(1-r_0)\left[-2rR_0+(1+r)\left|S_{\min,r}\right|\right]-(1+r_0)(1-r)\left|S_{\min,r}\right|}\left|S_{\min,r}\right|, & \left(r<-1 \text{ or } r>1,\ r_0<-1 \text{ or } r_0>1\right) \end{cases} \tag{13}$$

Substituting Eq. (13) into Eq. (7), the $s-n-R-d-r$ residual strength model considering the effect of stress ratio is determined as

$$\begin{cases} n=C\left\{\dfrac{2R_0^0\left(1-\alpha_1d^{\beta_1}\right)(1-r)S_{\max,r}}{(1-r_0)\left[2R_0^0\left(1-\alpha_1d^{\beta_1}\right)-(1+r)S_{\max,r}\right]+(1+r_0)(1-r)S_{\max,r}}\right. & \left(-1\le r\le 1,\ -1\le r_0\le 1\right) \\ \qquad \left.-S_0^0\left(1-\alpha_2d^{\beta_2}\right)\right\}^p\left[R_0^0\left(1-\alpha_1d^{\beta_1}\right)-R(n)\right]^q & \\ n=C\left\{\dfrac{-2r_0R_0^0\left(1-\alpha_1d^{\beta_1}\right)(1-r)\left|S_{\min,r}\right|}{(1-r_0)\left[-2rR_0^0\left(1-\alpha_1d^{\beta_1}\right)+(1+r)\left|S_{\min,r}\right|\right]-(1+r_0)(1-r)\left|S_{\min,r}\right|}\right. & \left(r<-1 \text{ or } r>1,\ r_0<-1 \text{ or } r_0>1\right) \\ \qquad \left.-S_0^0\left(1-\alpha_2d^{\beta_2}\right)\right\}^p\left[R_0^0\left(1-\alpha_1d^{\beta_1}\right)-R(n)\right]^q & \end{cases} \tag{14}$$

Obviously, Eq. (14) is a phenomenological model which can quantitatively characterize the effect of

notch depth and stress ratio on residual service life and residual strength of the composite component. Based on the initial residual strength data (d_i, R_{0i}) of un-notched and notched 3238A/EW250F and 3238A/CF3052 laminates obtained by static tensile and compressive static tests, the model constants α_1, β_1 and R_0^0 for tension and compression are determined by means of the linear regression principle. Again, using the T-T and C-C fatigue test data (s_i, n_i, R_i, d_i) of un-notched and notched 3238A/EW250F and 3238A/CF3052 laminates, the model parameters α_2, β_2, S_0^0, p, q and C at the given stress ratio r_0 of 0.05 and 10 in this paper are determined by best fitting method. Table 4 presents the $s-n-R-d-r$ residual strength models of 3238A/EW250F and 3238A/CF3052 woven composite laminates.

Note that, when both s and R equal the fatigue stress S, the number of loading cycles n should be the fatigue life N. The residual strength model in Table 4 will then be turned into the equations for the $S-N$ curves and the $s-n-R$ surfaces under given stress ratio and notch depth. The $S-N$ curves in Fig. 4 and the $s-n-R$ fatigue surfaces in Fig. 5 are plotted for the 3238A/EW250F and 3238A/CF3052 specimens at stress ratios of 0.05 and 10 with notch depth of 0, 2 mm, 3 mm and 4 mm, respectively. It can be seen from Figs. 4 and 5 that the predictions have good correlation with experimental results, demonstrating the validity of the $s-n-R-d-r$ residual strength model.

4.2. Fatigue life predictions for DEN specimen with 3mm notch depth

To demonstrate the application of the $s-n-R-d-r$ residual strength model developed in Section 4.1, fatigue lives of the DEN 3238A/EW250F and 3238A/CF3052 specimens with 3 mm double edge notches are predicted and compared with the experimental results. Palmgren–Miner rule, $s-n-R$ residual strength surface model and progressive damage analysis are used to predict the fatigue life of the notched specimen under block loading shown in Fig. 2.

Firstly, based on the $s-n-R-d-r$ residual strength models in Table 4, the $S-N$ curve models of 3238A/EW250F and 3238A/CF3052 laminates with 3 mm double edge notches are obtained and listed in Table 5. By utilizing them together with the Palmgren-Miner rule, the final fatigue life of composite laminates under block loading is determined when the cumulative Miner damage equals 1. Moreover, based on the developed $s-n-R-d-r$ residual strength models in Table 4, the $s-n-R$ residual strength surface models of 3238A/EW250F and 3238A/CF3052 laminates with 3 mm double edge notches are obtained and listed in Table 6. By using them, the strength of 3mm notched composite

laminates under block loading shown in Fig. 2 can be gradually degraded with increasing number of loading cycles. It is worth pointing out that for the load history containing both T-T and C-C fatigue loads, the ratio of residual strength to initial residual strength is used for degradation during fatigue process. According to the residual strength criterion: failure occurs when the applied stress equals the residual strength, the failure of composites is identified. Thus the fatigue lives of 3238A/EW250F and 3238A/CF3052 laminates with 3 mm double edge notches under block loading shown in Fig. 2 are obtained.

In addition, according to the flowchart in Fig. 12, the residual life and damage progression of composite structures under spectrum fatigue load can be evaluated through iterative cycles of FE stress analysis, material property degradation and failure identification. The FE model of 3 mm double edge notched composites with $[(45/-45)/(0/90)]_{3s}$ stacking sequence (shown in Fig. 1b) is established with commercial FE software ANSYS by SHELL181 element. The mesh around the notch is refined as shown in Fig. 13. There are 1776 elements in total. A mesh density study has been carried out to avoid the dependency of simulation result on mesh size. The mesh of the FE model was refined iteratively until the mesh size had negligible effect on the life prediction in the progressive damage analysis, as shown in Fig. 14. Note that M in Fig. 14 is the number of elements and N is the life prediction of 3238A/EW250F composite laminates with 3 mm double edge notches at the maximum fatigue stress of 125MPa under T-T loading. Basic mechanical properties of material in Table 1 are used for the model. The symmetry constraint is applied to the right side, the complete displacement constraint is applied to the bottom, and the fatigue load is applied to the top of the model. Then the stress state of each element can be calculated. Considering that the final fracture of notched composite laminates happens perpendicular to the loading direction as shown in Figs. 8 and 10 which is mainly controlled by the applied axial stress, the through-thickness equivalent stress component in Y axis is used for the progressive damage analysis. Based on the developed $s-n-R-d-r$ residual strength models in Table 4, the $s-n-R$ residual strength surface models of un-notched 3238A/EW250F and 3238A/CF3052 laminates are obtained and listed in Table 7, which are used for gradual material property degradation of elements. By using the residual strength criterion, the failed element is identified and the FE stress analysis is re-executed. In that way, the iterative cycles of FE stress analysis, material property degradation and failure identification are performed until the final failure of composite laminate happens, obtaining the residual life and damage propagation.

4.3. Comparison between experimental and numerical results

The residual life and damage propagation of the FE model under constant-amplitude fatigue loading at the stress ratios of 0.05 and 10 are illustrated in Figs. 15 and 16. In Fig. 15, the failed elements during fatigue process are marked with red color. Fig. 15a shows the damage propagation of 3238A/EW250F composite laminates with 3 mm double edge notches at maximum fatigue stress of 98MPa under T-T loading, whereas Fig. 15b presents the damage propagation of 3238A/EW250F laminates with 3 mm notches at minimum fatigue stress of -124MPa (maximum absolute stress of the fatigue cycle) under C-C loading. It can be seen from Figs. 15 and 16 that the number of failed elements increases with increasing number of loading cycles. The model prediction agrees with the experimental observations in general. The fatigue damage initiates at the corner of the U-notch due to the stress concentration and propagates in some angles towards the center of specimen, which is consistent with the experimental observations in Fig. 6. With the increasing number of loading cycles and the stress relaxation explained in Section 3.1, the fatigue damage tends to propagate in the plane perpendicular to the loading direction and fails at this weakest plane.

The damaged area during fatigue process under C-C fatigue load is larger than that under T-T fatigue load, which agrees with the experimental observations as shown in Figs. 8 and 10 in general. The local buckling usually happens under compressive fatigue load, causing larger delamination under C-C fatigue load compared with the T-T fatigue load. Moreover, the composite laminates under T-T fatigue load show fibre-dominated failure modes which has fracture surface perpendicular to the loading direction; however, the matrix-dominated failure of composites under C-C fatigue load usually happens in the angled shear plane which is larger than the cross-section area. The calculated damage propagation area in notched 3238A/EW250F and 3238A/CF3052 laminates are nevertheless similar as both materials have similar damage mechanisms and failure modes except for some details like coarser fracture surface for carbon fiber composites as shown in Figs. 8 and 10. It should also be noted that the current progressive damage analysis relies on equivalent engineering parameters for model prediction, which makes the direct detailed comparison of the damage area between the numerical and the experimental results impractical at present. Future work is required to incorporate various physical failure modes in the progressive damage analysis to simulate the micro failure mechanisms in composites more accurately.

Table 8 summarizes the comparison between life predictions by the three methods in Section 4.2 and experimental results under block loading shown in Fig. 2. It can be seen that (i) for Palmgren–Miner rule, the predicted fatigue life of woven composite laminates under L-H loading and H-L loading are the same; however, for the developed $s-n-R-d-r$ residual strength model and progressive damage analysis, the predicted fatigue life under L-H loading is shorter than that under H-L loading. This proves that Palmgren–Miner rule cannot consider the effect of load sequence while $s-n-R-d-r$ residual strength model and application of residual strength model into progressive damage analysis can effectively consider the effect of load sequence, which is consistent with findings in literature[32]. Under variable-amplitude fatigue loading, the accumulated damage (or strength degradation) of composite material at the former stage will affect the damage (or strength degradation) at the next stage, so using the residual strength model as fatigue damage metric can naturally take load sequence into consideration; (ii) the maximum relative deviations between experimental results and predictions by Palmgren–Miner rule, $s-n-R-d-r$ model and progressive damage analysis are 43.10%, 30.32% and 18.41%, respectively. The prediction based on Palmgren-Miner rule does not account for load sequence effect and has the lowest life prediction accuracy as compared with the experimental results. The progressive damage analysis has best prediction accuracy but the most complicated computational process. The $s-n-R-d-r$ residual strength model has lower (but reasonable) calculation accuracy than progressive damage analysis but is much simpler, demonstrating great potential for engineering application.

In order to further compare and discuss the damage accumulation under L-H and H-L loading, the damage accumulations of 3238A/EW250F composite laminates with 3mm double edge notches under L-H and H-L loading are predicted with Palmgren–Miner rule and $s-n-R$ residual strength (RS) surface model (shown in Fig. 17). Note that the cumulative damage index $D(n)$ corresponding to Palmgren-Miner rule is calculated by fatigue $S-N$ curve models in Table 5 and Eq. (3), while for the RS surface model it is calculated based on the $s-n-R$ surfaces in Table 6 as follows:

$$D(n)=1-\frac{R(n)\text{-}s}{R_0-s} \tag{15}$$

It can be seen from Fig. 17 that the cumulative Miner damages under L-H and H-L loading follow a linear rule and reach 1 at the same number of fatigue loading cycles, indicating that Palmgren–Miner rule cannot account for load sequence effect. Unlike the cumulative Miner damage, for the RS surface

model, the cumulative damages follow a non-linear rule and is strongly dependent on the load sequence. Under L-H block loading, there exists a sudden acceleration of RS damage accumulation at the transition from first low stress block to second high stress block which follows higher damage accumulation rate. However, the transition from first high stress block to second low stress block under H-L loading causes an obvious retardation of RS damage accumulation with subsequent lower damage accumulation rate. As a result, the L-H load sequence is more damaging than H-L load sequence, which agrees with the experimental results discussed in Section 3.2.

5. CONCLUSIONS

This paper presents an experimental and numerical study of the notch effect on strength and fatigue life of DEN composite laminate specimen made of woven glass fibre lamina 3238A/EW250F and wove carbon fibre lamina 3238A/CF3052 under tensile and compressive static load, constant-amplitude T-T (R=0.05) and C-C (R=10) fatigue load, and H-L, L-H, and H-L-H block fatigue load. Following conclusions can be drawn from the experimental and numerical results obtained in the study:

(i) The double edge notches have significant detrimental effect on static and fatigue strength of woven composite laminates. The detrimental effect is greater under tensile static and fatigue load than compressive static and fatigue load.

(ii) The fatigue damage of woven composite laminates is significantly affected by load sequence. The L-H block load is more damaging than H-L block load. The transitions between tensile stress block and compressive stress block can significantly shorten the fatigue life of woven composite laminates.

(iii) The fatigue damage mechanisms of un-notched and notched woven composite laminates are similar. The damage mechanisms under T-T and C-C fatigue load are however significantly different. The fatigue specimens under T-T fatigue load show fibre-dominated failure modes while those under C-C fatigue load are controlled by matrix-dominated failure modes. Moreover, the fatigue damage in 3238A/CF3052 composites is more severe than that in 3238A/EW250F composites.

(iv) A $s-n-R-d-r$ residual strength model considering the effect of notch depth and stress ratio and progressive damage algorithm has been developed to predict fatigue lives of notched woven composite laminates. Good agreement between the experimental results and the numerical predictions has been achieved, demonstrating the validity and great potential for engineering applications of the numerical model and the progressive damage algorithm developed in the current study.

Appendix A

Taking the logarithm form of Eq. (5) yields

$$u = a + bv \tag{A-1}$$

with

$$u = \lg(\frac{R_0^0 - R_0}{R_0^0}) \tag{A-2}$$

$$v = \lg d \tag{A-3}$$

$$a = \lg \alpha_1 \tag{A-4}$$

$$b = \beta_1 \tag{A-5}$$

By means of the linear regression principle, the undetermined parameters a and b can be obtained. Then α_1 and β_1 are determined and the function can be obtained as follows.

$$\alpha_1 = 10^{(\overline{u} - \beta_1 \overline{v})} \tag{A-6}$$

$$\beta_1 = \frac{L_{vu}}{L_{vv}} \tag{A-7}$$

where

$$\begin{cases} \overline{v} = \dfrac{1}{n}\sum_{i=1}^{n} v_i \\ \overline{u} = \dfrac{1}{n}\sum_{i=1}^{n} u_i \\ L_{vv} = \sum_{i=1}^{n} \left(v_i - \overline{v}\right)^2 \\ L_{vu} = \sum_{i=1}^{n} \left(v_i - \overline{v}\right)\left(u_i - \overline{u}\right) \end{cases} \tag{A-8}$$

Appendix B

Taking the logarithm form of Eq. (7) yields

$$y = a_0 + a_1 x_1 + a_2 x_2 \tag{B-1}$$

with

$$y = \lg n \tag{B-2}$$

$$x_1 = \lg\left[s - S_0^0 (1 - \alpha_2 d^{\beta_2}) \right] \tag{B-3}$$

$$x_2 = \lg\left\{ R_0^0 \left[1 - 10^{(\bar{u} - \beta_1 \bar{v})} \cdot d^{\frac{L_{vu}}{L_{vv}}} \right] - R(n) \right\} \tag{B-4}$$

$$a_0 = \lg C \tag{B-5}$$

$$a_1 = p \tag{B-6}$$

$$a_2 = q \tag{B-7}$$

According to the maximum likelihood principle, the constants a_0, a_1, a_2 and residual sum of squares Q can be obtained

$$a_0 = \bar{y} - a_1 \bar{x}_1 - a_2 \bar{x}_2 \tag{B-8}$$

$$a_1 = \frac{L_{12} L_{20} - L_{22} L_{10}}{L_{12} L_{21} - L_{11} L_{22}} \tag{B-9}$$

$$a_2 = \frac{L_{21} L_{10} - L_{11} L_{20}}{L_{12} L_{21} - L_{11} L_{22}} \tag{B-10}$$

$$Q = \sum_{i=1}^{l} \left(y_i - a_0 - a_1 x_1 - a_2 x_2 \right)^2 \tag{B-11}$$

where

$$\begin{cases} \overline{y} = \dfrac{1}{l}\sum_{i=1}^{l} y_i \\ \overline{x}_1 = \dfrac{1}{l}\sum_{i=1}^{l} x_{1i} \\ \overline{x}_2 = \dfrac{1}{l}\sum_{i=1}^{l} x_{2i} \\ L_{11} = \sum_{i=1}^{l}\left(x_{1i} - \overline{x}_1\right)^2 \\ L_{22} = \sum_{i=1}^{l}\left(x_{2i} - \overline{x}_2\right)^2 \\ L_{12} = L_{21} = \sum_{i=1}^{l}\left(x_{1i} - \overline{x}_1\right)\left(x_{2i} - \overline{x}_2\right) \\ L_{10} = \sum_{i=1}^{l}\left(x_{1i} - \overline{x}_1\right)\left(y_i - \overline{y}\right) \\ L_{20} = \sum_{i=1}^{l}\left(x_{2i} - \overline{x}_2\right)\left(y_i - \overline{y}\right) \end{cases} \tag{B-12}$$

From the above equations, it can be seen that $\overline{x}_1$, L_{11}, L_{12} and L_{10} are functions of the undetermined constants S_0^0, α_2 and β_2. So the undetermined parameters a_0, a_1, a_2 and Q are also the functions with regard to S_0^0, α_2 and β_2. By means of the minimum value principle of $Q(S_0^0, \alpha_2, \beta_2)$, it is possible to have the solving equations with regard to S_0^0, α_2 and β_2.

$$\begin{cases} \dfrac{\partial Q}{\partial S_0^0} = 0 \\ \dfrac{\partial Q}{\partial \alpha_2} = 0 \\ \dfrac{\partial Q}{\partial \beta_2} = 0 \end{cases} \tag{B-13}$$

By numerically solving Eq. (B-7), the solutions of S_0^0, α_2 and β_2 can be obtained and the unknown constants p, q and C are then determined as

$$p = \frac{L_{12}L_{20} - L_{22}L_{10}}{L_{12}L_{21} - L_{11}L_{22}} \tag{B-14}$$

$$q = \frac{L_{21}L_{10} - L_{11}L_{20}}{L_{12}L_{21} - L_{11}L_{22}} \tag{B-15}$$

$$C = 10^{(\bar{y} - a_1\bar{x}_1 - a_2\bar{x}_2)} \tag{B-16}$$

ACKNOWLEDGEMENTS

This project was supported by the National Natural Science Foundation of China (Grant No. 51875021).

REFERENCES

[1] Xu W, Thorsson SI, Waas AM. Experimental and numerical study on cross-ply woven textile composite with notches and cracks[J]. Composite Structures, 2015, 132:816-824.

[2] Mall S, Boyer BH. Cyclic and sustained loading behaviors of oxide/oxide Nextel™ 720/alumina composite with double edge sharp notch[J]. Composites Part A Applied Science & Manufacturing, 2012, 43(43):1153–1159.

[3] Muc A, Romanowicz P. Effect of notch on static and fatigue performance of multilayered composite structures under tensile loads[J]. Composite Structures, 2017, 178:27-36.

[4] Beyene AT, Belingardi G, Koricho EG. Effect of notch on quasi-static and fatigue flexural performance of Twill E-Glass/Epoxy composite[J]. Composite Structures, 2016, 153:825-842.

[5] Khashaba UA, Selmy AI, El-Sonbaty IA, Megahed M. Behavior of notched and unnotched [0/±30/±60/90] s GFR/EPOXY composites under static and fatigue loads[J]. Composite structures, 2007, 81(4): 606-613.

[6] Kawai M, Shiratsuchi T. Vanishing notch sensitivity approach to fatigue life prediction of notched cross-ply CFRP laminates at room temperature[J]. Journal of Composite Materials, 2012, 46(23): 2935-2950.

[7] Dai S, Cunningham PR, Marshall S, Silva C. Open hole quasi-static and fatigue characterisation of 3D woven composites[J]. Composite Structures, 2015, 131:765-774.

[8] Alderliesten RC. Critical review on the assessment of fatigue and fracture in composite materials and structures[J]. Engineering Failure Analysis, 2013, 35:370-379.

[9] Aidi B, Philen MK, Case SW. Progressive damage assessment of centrally notched composite specimens in fatigue[J]. Composites Part A: Applied Science and Manufacturing, 2015, 74:47-59.

[10] Vieille B, Albouy W. Fatigue damage accumulation in notched woven-ply thermoplastic and

thermoset laminates at high-temperature: Influence of matrix ductility and fatigue life prediction[J]. International Journal of Fatigue, 2015, 80:1-9.

[11] Nixon-Pearson OJ, Hallett SR. An investigation into the damage development and residual strengths of open-hole specimens in fatigue[J]. Composites Part A, 2015, 69(2):266-278.

[12] Broughton WR, Gower MRL, Lodeiro MJ, Pilkington GD, Shaw RM. National Physical. An experimental assessment of open-hole tension–tension fatigue behaviour of a GFRP laminate[J]. Composites Part A: Applied Science and Manufacturing, 2011, 42(10): 1310-1320.

[13] Xiong JJ, Shenoi RA . General aspects on structural integrity[J]. Chinese Journal of Aeronautics, 2019, 32(1): 114-132.

[14] Post NL, Case SW, Lesko JJ. Modeling the variable amplitude fatigue of composite materials: A review and evaluation of the state of the art for spectrum loading[J]. International Journal of Fatigue, 2008, 30(12): 2064-2086.

[15] Found MS, Quaresimin M. Two-stage fatigue loading of woven carbon fibre reinforced laminates[J]. Fatigue & Fracture of Engineering Materials & Structures, 2003, 26(1):17-26.

[16] Sarfaraz R, Vassilopoulos AP , Keller T . Block loading fatigue of adhesively bonded pultruded GFRP joints[J]. International Journal of Fatigue, 2013, 49:40-49.

[17] Epaarachchi JA. A study on estimation of damage accumulation of glass fibre reinforce plastic (GFRP) composites under a block loading situation[J]. Composite Structures, 2006, 75(1-4):88-92.

[18] Paepegem WV. Fatigue models for woven textile composite laminates[M]. Fatigue of Textile Composites. 2015.

[19] Philippidis TP, Passipoularidis VA. Residual strength after fatigue in composites: Theory vs. experiment[J]. International Journal of Fatigue, 2007, 29(12):2104-2116.

[20] Chen XJ, Sun Y, Wu ZW, Yao LJ, Zhang YL, Zhou S, Liu YZ. An investigation on residual strength and failure probability prediction for plain weave composite under random fatigue loading[J]. International Journal of Fatigue, 2019, 120: 267-282.

[21] Sidoroff F, Subagio B. Fatigue damage modeling of composite materials from bending test. In: Matthews F L, Buskell N C R, Hodgkinson J M，Morton J (eds), 6th International Conference on Composite Materials(ICCM—VI) & Second European Conference on Composite Materials (ECCM—II): 4. Proceeding, London, UK, Elsevier, 1987, 4: 32-39.

[22] Whitworth HA. A stiffness degradation model for composite laminates under fatigue loading[J].

Composite Structures, 1997, 40(2):95-101.

[23] Yang JN, Jones DL, Yang SH, Meskini A. A stiffness Degradation Model for Graphite/Epoxy Laminates[J]. Journal of Composite Materials, 1990, 24(7):753-769.

[24] Paepegem WV, Degrieck J. Experimental set-up for and numerical modelling of bending fatigue experiments on plain woven glass/epoxy composites[J]. Composite Structures, 2001, 51(1):1-8.

[25] Tate JS, Kelkar AD. Stiffness degradation model for biaxial braided composites under fatigue loading[J]. Composites Part B: Engineering, 2008, 39(3):548-555.

[26] Yao L, Rong Q, Shan ZD, Qiu YP. Static and bending fatigue properties of ultra-thick 3D orthogonal woven composites[J]. Journal of Composite Materials, 2013, 47(5):569-577.

[27] Yoshioka K, Seferis JC. Modeling of tensile fatigue damage in resin transfer molded woven carbon fabric composites[J]. Composites Part A: Applied Science and Manufacturing, 2002, 33(11):1593-1601.

[28] Shokrieh MM, Lessard LB. Progressive Fatigue Damage Modeling of Composite Materials, Part I: Modeling[J]. Journal of Composite Materials, 2000, 34(13):1056-1080.

[29] Shokrieh MM, Lessard LB. Progressive Fatigue Damage Modeling of Composite Materials, Part II: Material Characterization and Model Verification[J]. Journal of Composite Materials, 2000, 34(13):1081-1116.

[30] Lian W, Yao WX. Fatigue life prediction of composite laminates by FEA simulation method[J]. International Journal of Fatigue, 2010, 32(1):123-133.

[31] Eliopoulos EN, Philippidis TP. A progressive damage simulation algorithm for GFRP composites under cyclic loading. Part I: Material constitutive model[J]. Composites Science & Technology, 2011, 71(5):742-749.

[32] Eliopoulos EN, Philippidis TP. A progressive damage simulation algorithm for GFRP composites under cyclic loading. Part II: FE implementation and model validation[J]. Composites Science & Technology, 2011, 71(5):750-757.

[33] Passipoularidis VA, Philippidis TP, Brondsted P. Fatigue life prediction in composites using progressive damage modelling under block and spectrum loading[J]. International Journal of Fatigue, 2011, 33(2): 132-144.

[34] Wicaksono S, Chai GB. Life prediction of woven CFRP structure subject to static and fatigue loading[J]. Composite Structures, 2015, 119:185-194.

[35] Hochard C, Thollon Y. A generalized damage model for woven ply laminates under static and fatigue loading conditions[J]. International Journal of Fatigue, 2010, 32(1):158-165.

[36] Xu J, Lomov SV, Verpoest I, Daggumati S, Paepegem WV, Degrieck J. A progressive damage model of textile composites on meso-scale using finite element method: Fatigue damage analysis[J]. Computers & Structures, 2015, 152(25):96-112.

[37] Xu J, Lomov SV, Verpoest I, Daggumati S, Paepegem WV, Degrieck J. A comparative study of twill weave reinforced composites under tension–tension fatigue loading: Experiments and meso-modelling[J]. Composite Structures, 2016, 135:306-315.

[38] ASTM D5766-11. Standard test method for open-hole tensile strength of polymer matrix composite laminates[J]. 2011.

[39] ASTM D6484-09. Standard test method for open-hole compressive strength of polymer matrix composite laminates[J]. 2009.

[40] ASTM D7615-11. Standard practice for open-hole fatigue response of polymer matrix composite laminates[J]. 2011.

[41] ASTM E739-10. Standard practice for statistical analysis of linear or linearized stress-life (s-n) and strain-life (ε-n) fatigue data1[J]. 2010.

[42] Sandor BI. Fundamentals of cyclic stress and strain[M]. Univ of Wisconsin Pr, 1972.

[43] Liu HT, Xiong JJ, Gao ZT. Fatigue test on α value in Miner linear accumulated damage theory[J]. Mechanics in Engineering, 2002, 24(4):52-55.

[44] Schaff JR, Davidson BD. Life prediction methodology for composite structures. Part I—Constant amplitude and two-stress level fatigue[J]. Journal of composite materials, 1997, 31(2): 128-157.

[45] Opelt CV, Paiva JMF, Candido GM, Rezende MC. A fractographic study on the effects of hygrothermal conditioning on carbon fiber/epoxy laminates submitted to axial compression[J]. Engineering Failure Analysis, 2017, 79: 342-350.

[46] Opelt CV, Candido GM, Rezende MC. Compressive failure of fiber reinforced polymer composites–a fractographic study of the compression failure modes[J]. Materials Today Communications, 2018, 15: 218-227.

[47] Gorbatikh L, Lomov SV. Damage accumulation in textile composites[M]. Modeling Damage, Fatigue and Failure of Composite Materials. 2016: 41-59.

[48] Xiong JJ, Shenoi RA. Two new practical models for estimating reliability-based fatigue strength

of composites[J]. Journal of composite materials, 2004, 38(14): 1187-1209.

[49] Goodman J. Mechanics applied to engineering. Harlow, UK: Longman Green; 1899.

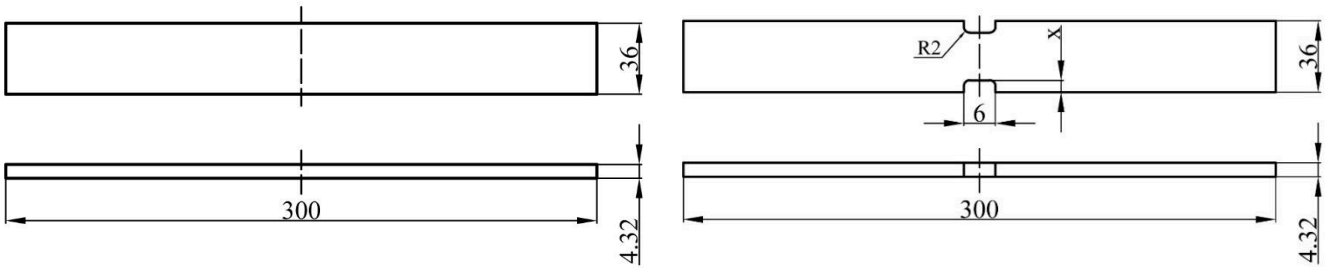

(a) Un-notched specimen (b) Notched specimen

Fig. 1 Geometric configuration and dimensions of specimen.

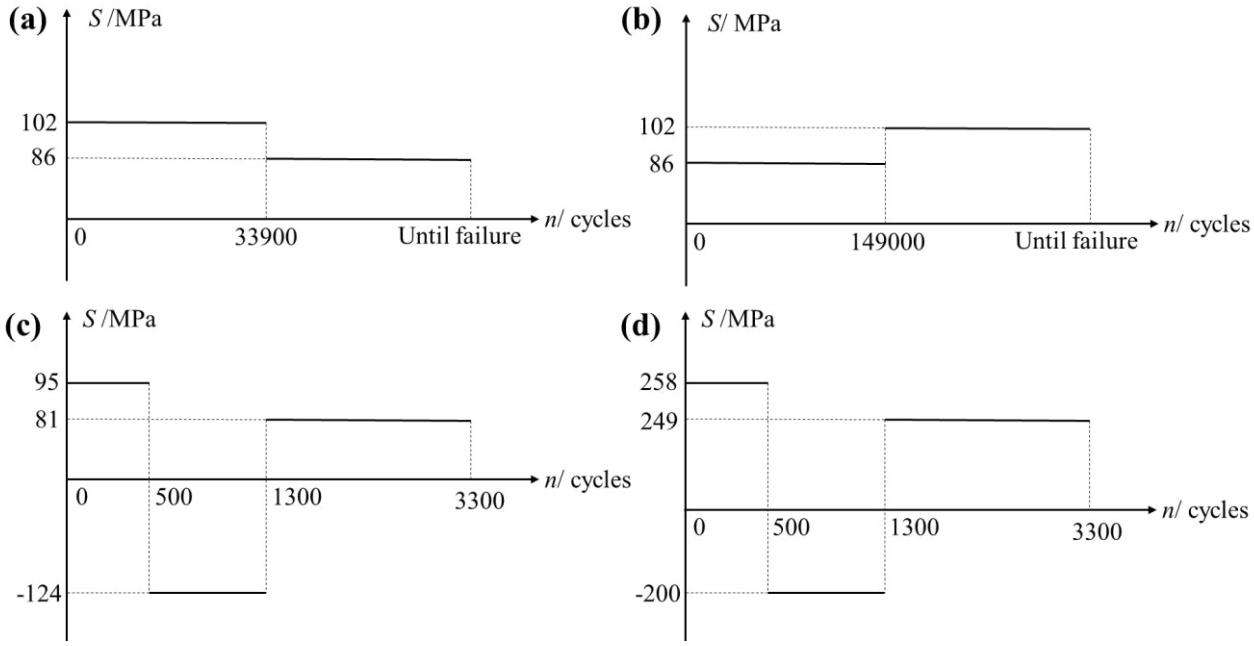

Fig. 2 Load history of block-loading fatigue tests: (a) H-L load history for 3238A/EW250F laminates, (b) L-H load history for 3238A/EW250F laminates, (c) H-L-H load history for 3238A/EW250F laminates, (d) H-L-H load history for 3238A/CF3052 laminates.

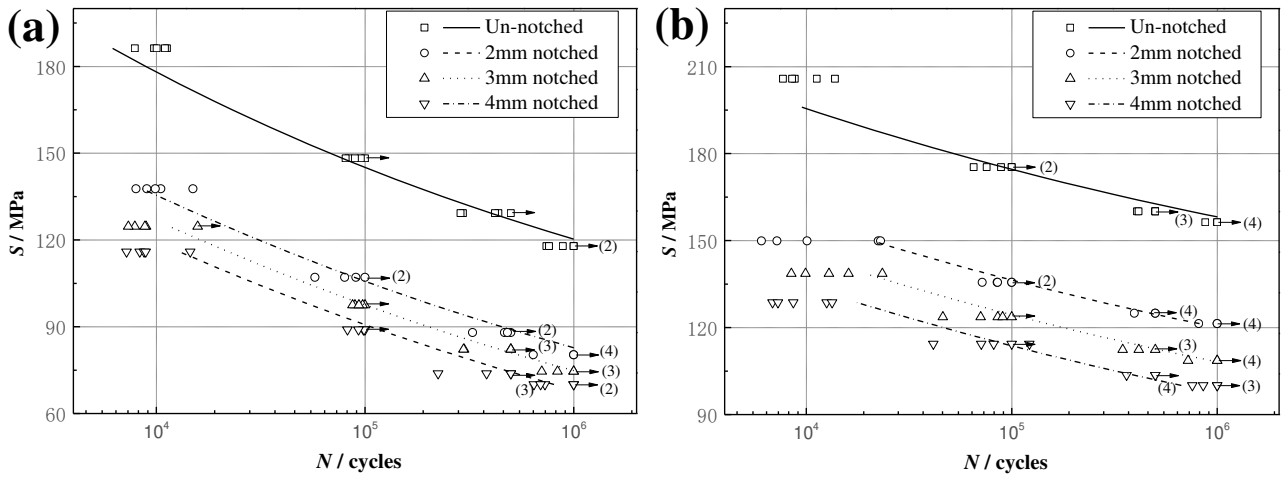

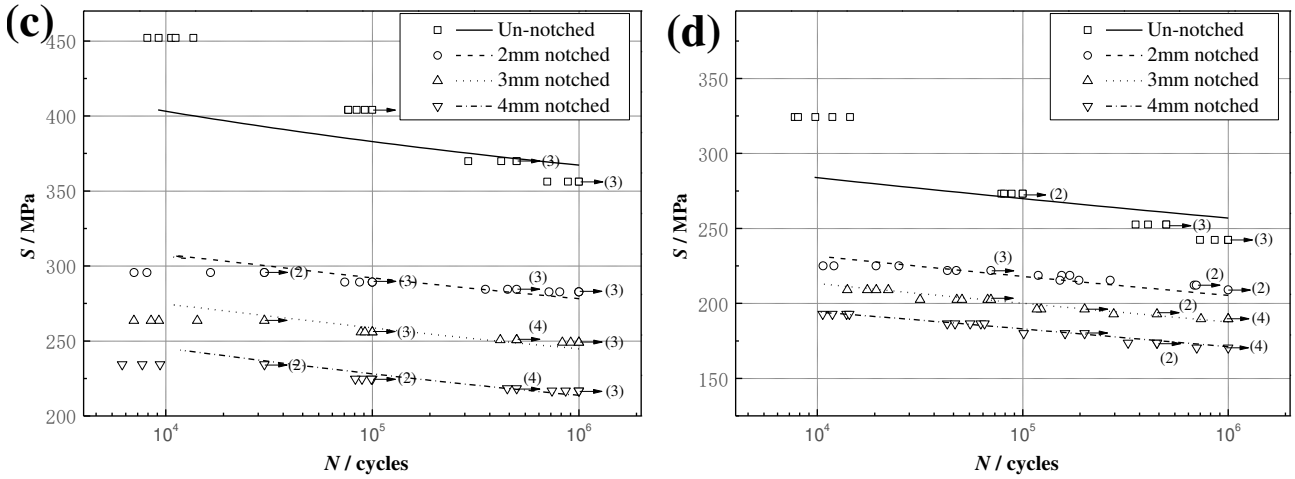

Fig. 3 Constant-amplitude fatigue test results: (a) 3238A/EW250F at the stress ratio of 0.05 (T-T), (b) 3238A/EW250F at the stress ratio of 10 (C-C), (c) 3238A/CF3052 at the stress ratio of 0.05 (T-T), (d) 3238A/ CF3052 at the stress ratio of 10 (C-C).

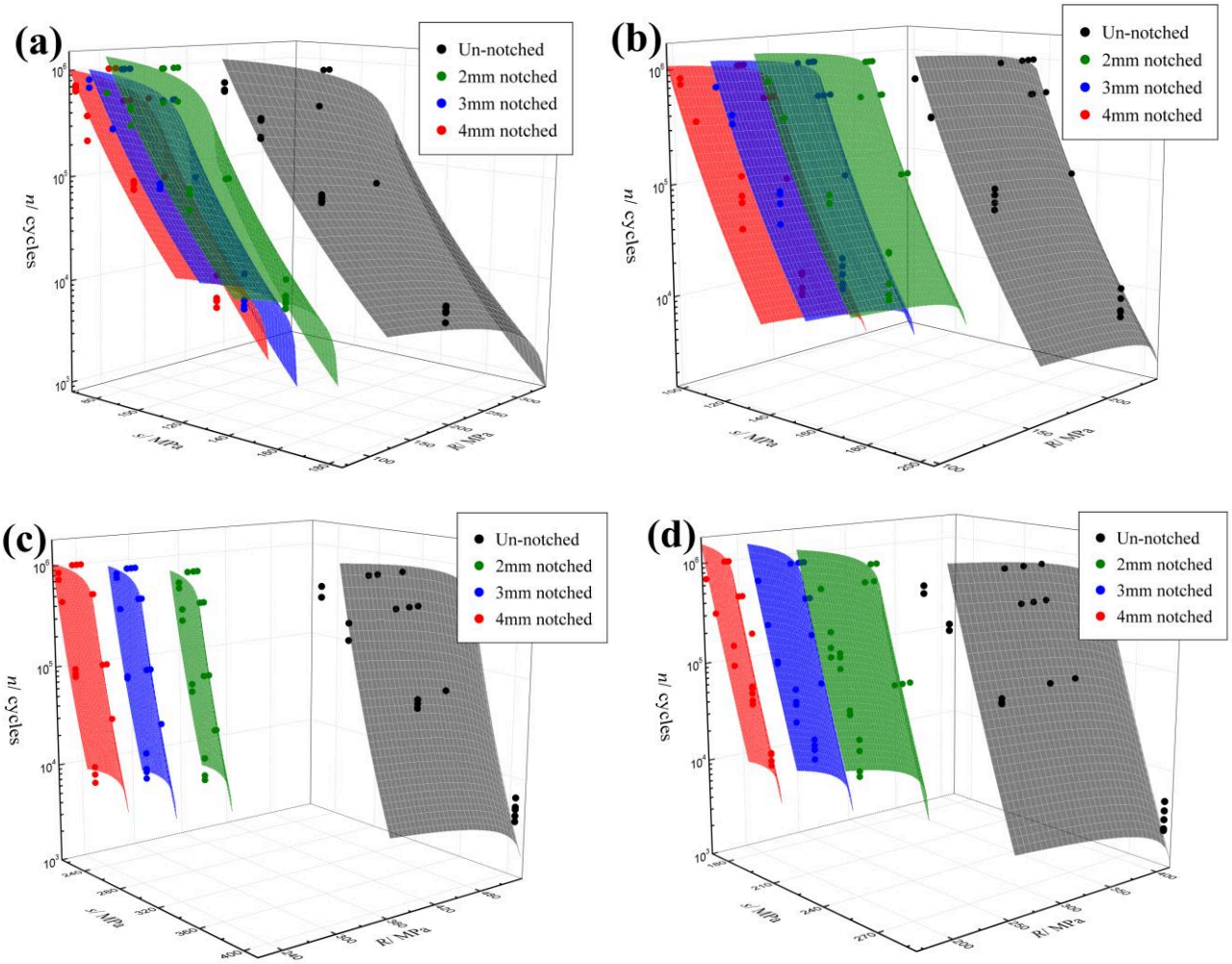

Fig. 4 Fatigue $s-n-R$ surfaces: (a) 3238A/EW250F at the stress ratio of 0.05 (T-T), (b) 3238A/EW250F at the stress ratio of 10 (C-C), (c) 3238A/CF3052 at the stress ratio of 0.05 (T-T), (d) 3238A/ CF3052 at the stress ratio of 10 (C-C).

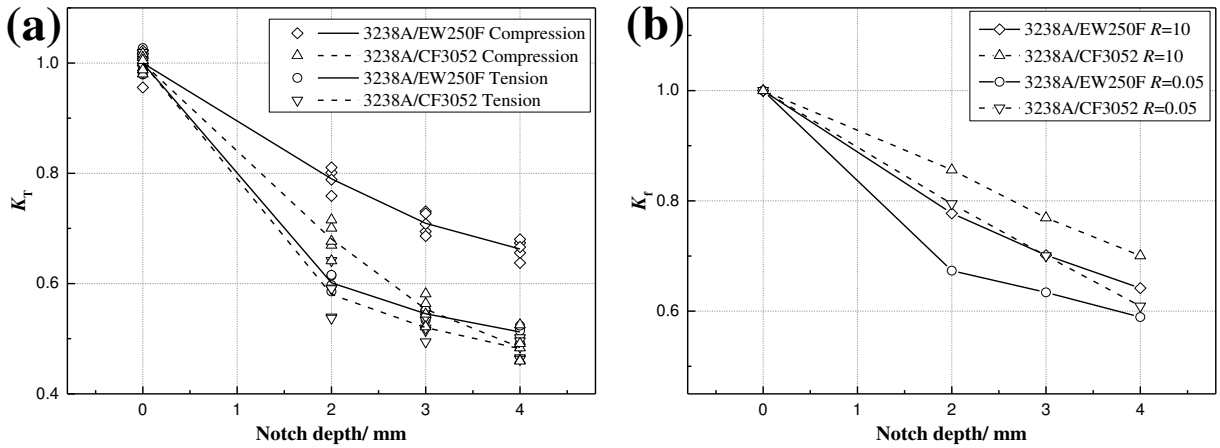

Fig. 5 Strength reduction and notch factor curves: (a) variation of strength reduction factor with notch depth, (b) variation of the notch factor with notch depth at the nominal fatigue life of 10^6 cycles.

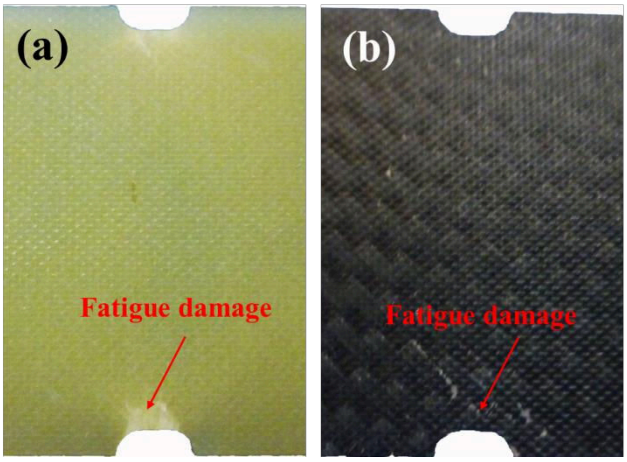

Fig. 6 Macro photographs of damaged composite specimens: (a) notched 3238A/EW250F specimen, (b) notched 3238A/CF3052 specimen.

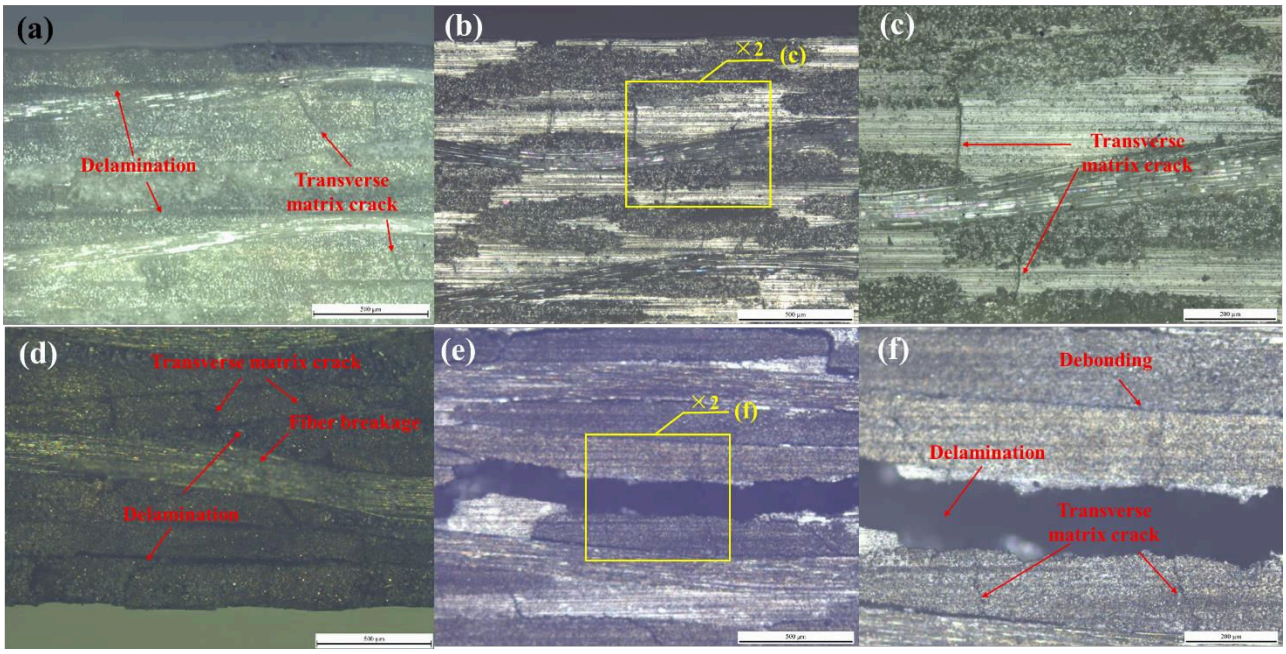

Fig. 7 Fatigue damages at the edge of run-out specimens at 10^6 loading cycles under T-T fatigue load: (a) notched 3238A/EW250F specimen, (b)(c) un-notched 3238A/EW250F specimen, (d) notched 3238A/CF3052 specimen, (e)(f) un-notched 3238A/CF3052 specimen.

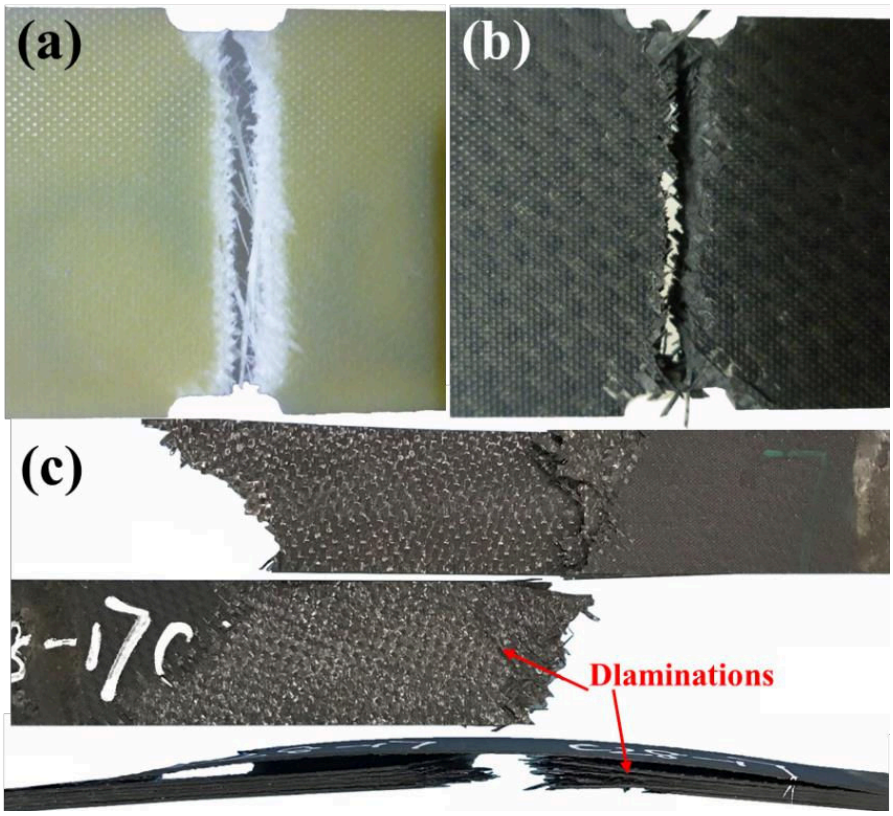

Fig. 8 Failure modes of specimens under T-T fatigue load: (a) notched 3238A/EW250F specimen, (b) notched 3238A/CF3052 specimen, (c) un-notched 3238A/CF3052 specimen.

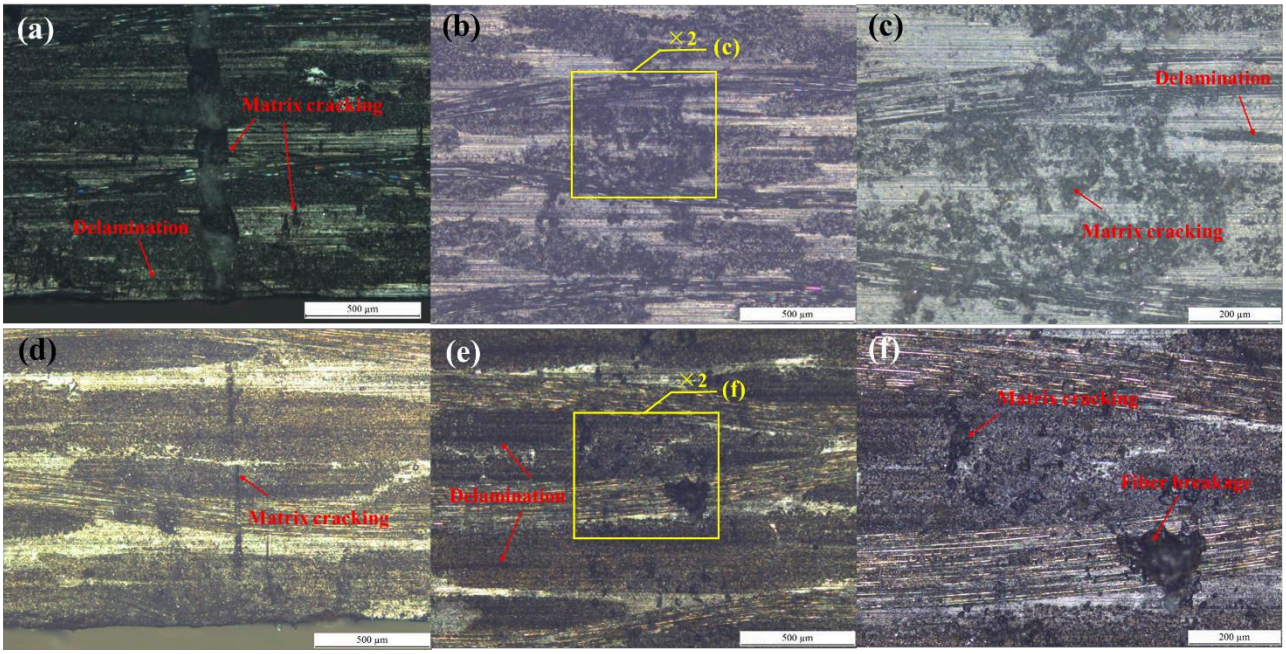

Fig. 9 Fatigue damage at the edge of run-out specimens at 10^6 loading cycles under C-C fatigue

load: (a) notched 3238A/EW250F specimen, (b)(c) un-notched 3238A/EW250F specimen, (d) notched 3238A/CF3052 specimen, (e)(f) un-notched 3238A/CF3052 specimen.

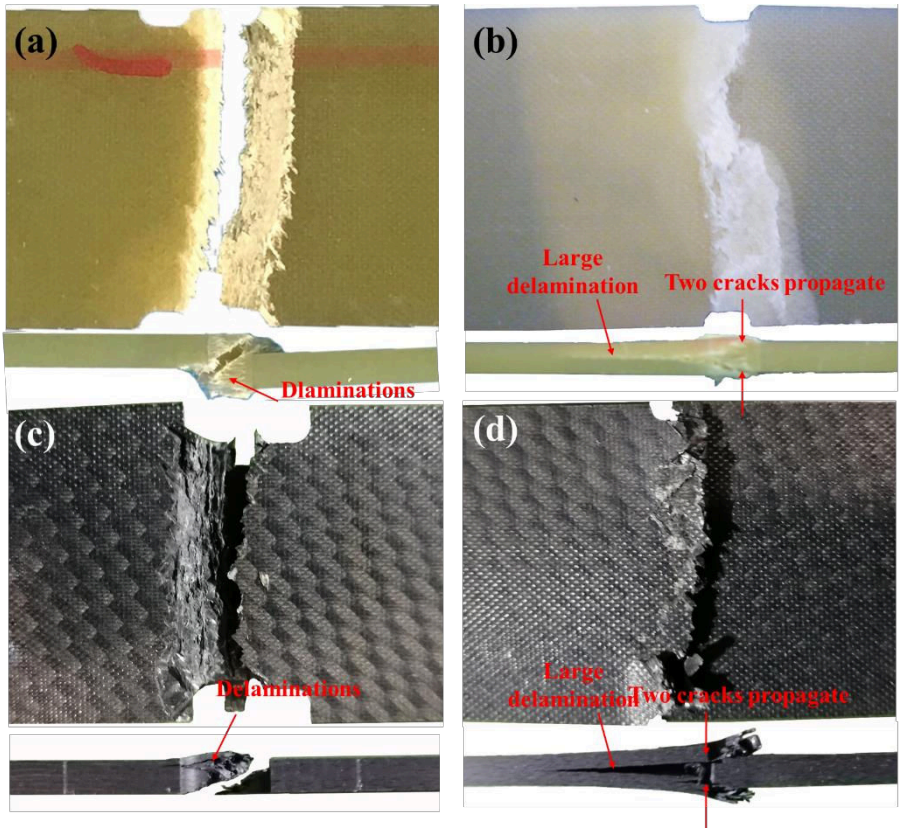

Fig. 10 Failure modes of notched specimens under C-C fatigue load: (a) mixed through-thickness shear and interlamilar failure mode of 3238A/EW250F specimen, (b) mixed wedge splitting and interlaminar failure mode of 3238A/EW250F specimen, (c) mixed through-thickness shear and interlamilar failure mode of 3238A/CF3052 specimen, (d) mixed wedge splitting and interlaminar failure mode of 3238A/CF3052 specimen.

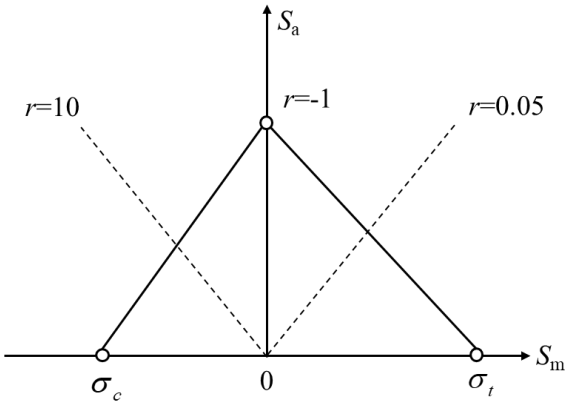

Fig. 11 Constant life diagram to account for stress ratio effect.

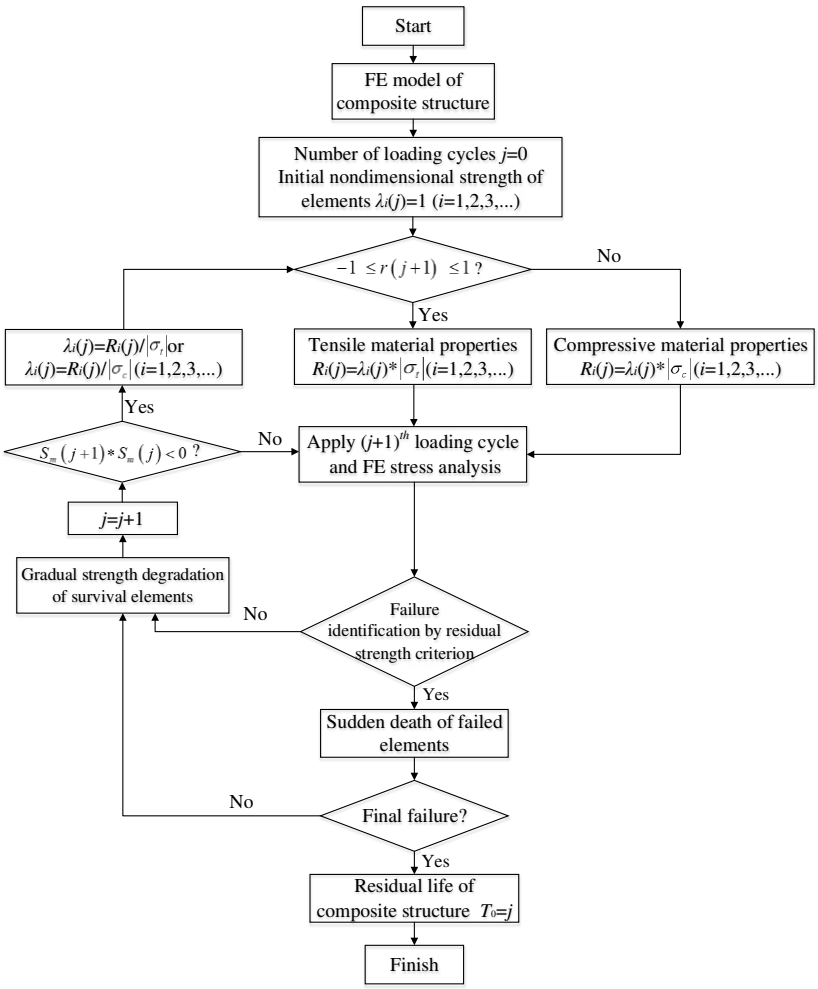

Fig. 12 Flowchart of progressive damage algorithm under spectrum fatigue loading.

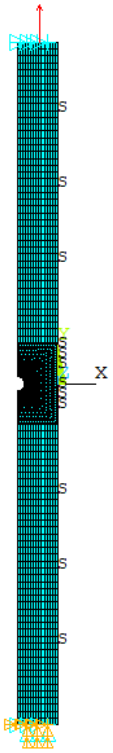

Fig. 13 Boundary conditions on FE model.

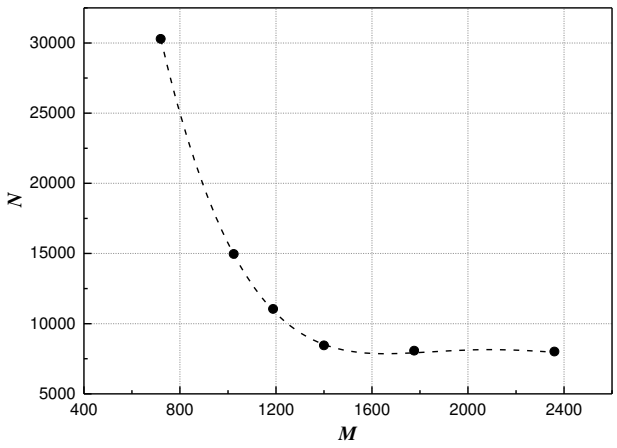

Fig. 14 Mesh density effect.

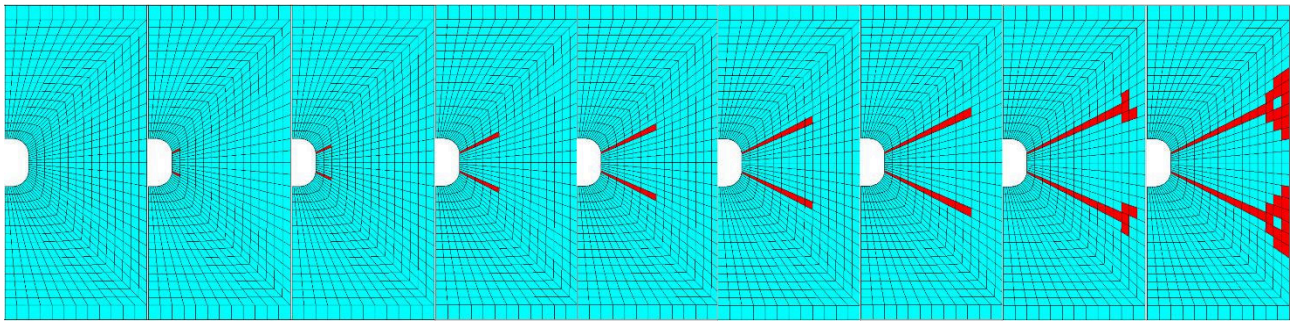

(a) Stress ratio of 0.05, fatigue stress of 98MPa

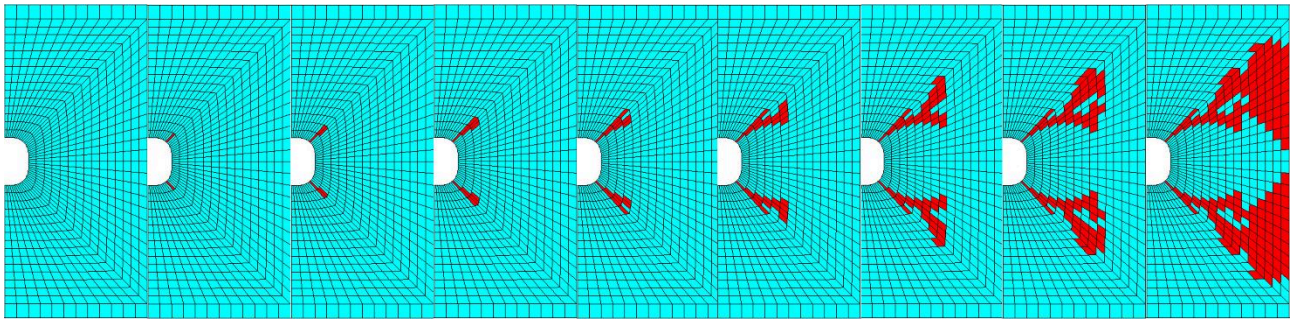

(b) Stress ratio of 10, fatigue stress of -124MPa

Fig. 15 Damage propagation in 3 mm notched 3238A/EW250F and 3238A/CF3052 laminates.

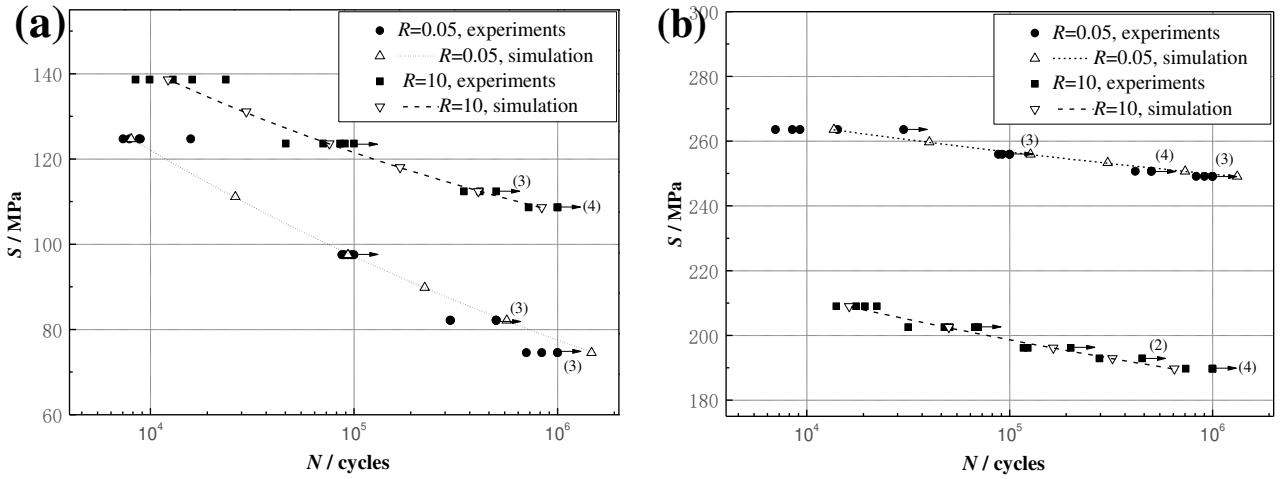

Fig. 16 Residual life predictions at the stress ratios of 0.05 and 10: (a) 3238A/EW250F composites, (b) 3238A/ CF3052 composites.

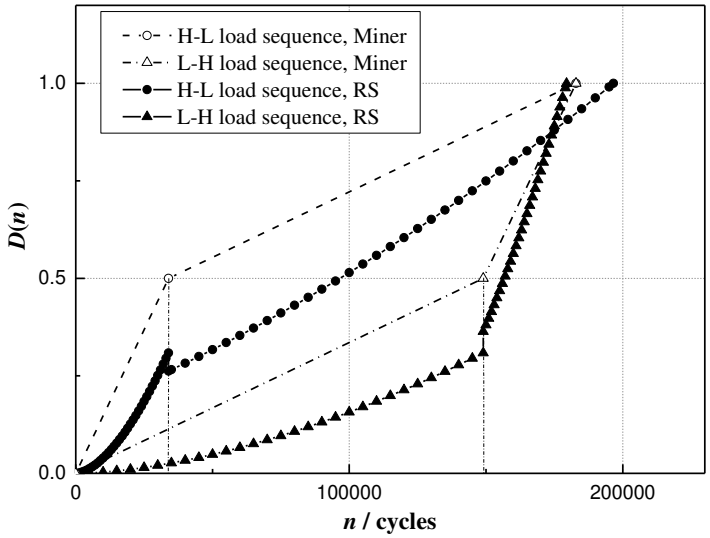

Fig. 17 Damage accumulation of 3238A/EW250F composites under L-H and H-L loading.

Table 1 Mechanical properties of 3238A/EW250F and 3238A/CF3052 composites.

Composites	Load direction	E_1 / GPa	E_2 / GPa	μ_{12}	σ_1 / MPa	σ_2 / MPa	G_{12} / GPa	G_{13} / GPa	G_{23} / GPa
3238A/ EW250F	Tension	17.77	17.71	0.11	361.9	364.5	1.72	1.13	1.13
	Compression	22.66	22.43	0.11	262.5	268.9	1.72	1.13	1.13
3238A/ CF3052	Tension	65.97	65.59	0.083	558.2	569.9	2.08	1.89	1.89
	Compression	51.03	51.21	0.083	511.6	512.7	2.08	1.89	1.89

Table 2 Static strengths of un-notched and notched laminates (unit: MPa).

Composites	Load direction	0	2mm	3mm	4mm
3238A/EW250F	Tension	349.5	210.2	190.5	179.0
	Compression	235.6	186.1	167.1	156.1
3238A/CF3052	Tension	541.8	314.3	281.9	261.2
	Compression	417.6	284.4	231.2	202.2

Table 3 Experimental results under block spectrum loading

Composites	Spectrum type	Fatigue life	Mean value	Cumulative damage	Mean value
3238A/EW250F	H-L	291630	228664	1.36	1.15

		215783		1.11	
		178580		0.99	
		161805		0.69	
	L-H	170493	170820	0.82	0.82
		180163		0.96	
		152232		0.72	
		165410		0.78	
	H-L-H	176036	158271	0.83	0.75
		158795		0.75	
		138884		0.66	
		159198		0.79	
		129601		0.65	
3238A/CF3052	H-L-H	149254	139276	0.74	0.69
		138983		0.69	
		119342		0.60	

Table 4 $s-n-R-d-r$ residual strength models.

Composites	Stress ratio	$s-n-R-d-r$ model
3238A/ EW250F	$-1 \le r \le 1$	$n=9.75\times10^{17}\left\{\frac{698.90\left(1-0.33d^{0.29}\right)(1-r)}{0.95\left[698.90\left(1-0.33d^{0.29}\right)-(1+r)s\right]+1.05(1-r)s}s-51.43\left(1-0.48d^{0.49}\right)\right\}^{-7.28}\left[349.45\left(1-0.33d^{0.29}\right)-R(n)\right]^{0.59}$
	$r<-1$ or $r>1$	$n=1.13\times10^{21}\left\{\frac{4712.0\left(1-0.13d^{0.69}\right)(1-r)}{-9\left[471.20r\left(1-0.13d^{0.69}\right)-(1+r)s\right]+11(1-r)s}s-102.32\left(1-0.23d^{0.67}\right)\right\}^{-8.79}\left[235.60\left(1-0.13d^{0.69}\right)-R(n)\right]^{0.16}$
3238A/ CF3052	$-1 \le r \le 1$	$n=4.35\times10^{20}\left\{\frac{1083.64\left(1-0.34d^{0.30}\right)(1-r)}{0.95\left[1083.64\left(1-0.34d^{0.30}\right)-(1+r)s\right]+1.02(1-r)s}s-313.38\left(1-0.16d^{0.81}\right)\right\}^{-8.87}\left[541.82\left(1-0.34d^{0.30}\right)-R(n)\right]^{0.32}$

$r<-1$ or $r>1$	$n=4.60\times10^{69}\left\{\dfrac{8352.6\left(1-0.20d^{0.70}\right)(1-r)}{-9\left[835.26r\left(1-0.20d^{0.70}\right)-(1+r)s\right]+11(1-r)s}s\right.$ $\left.-97.35\left(1-0.31d^{0.72}\right)\right\}^{-29.20}\left[417.63\left(1-0.20d^{0.70}\right)-R(n)\right]^{0.30}$

Table 5 Fatigue $S-N$ curves of laminates with 3mm double edge notches.

Composites	Stress ratio	$S-N$ curve
3238A/EW250F	0.05	$N=9.75\times10^{17}\left(S-9.58\right)^{-7.28}\left(192.01-S\right)^{0.59}$
	10	$N=1.13\times10^{21}\left(S-52.58\right)^{-8.79}\left(169.22-S\right)^{0.16}$
3238A/CF3052	0.05	$N=4.35\times10^{20}\left(S-193.85\right)^{-8.87}\left(283.69-S\right)^{0.32}$
	10	$N=4.60\times10^{69}\left(S-29.98\right)^{-29.20}\left(237.81-S\right)^{0.30}$

Table 6 Fatigue $s-n-R$ surface models of laminates with 3 mm double edge notches.

Composites	Stress ratio	$s-n-R$ surface
3238A/EW250F	0.05	$n=9.75\times10^{17}\left(s-9.58\right)^{-7.28}\left[192.01-R(n)\right]^{0.59}$
	10	$n=1.13\times10^{21}\left(s-52.58\right)^{-8.79}\left[169.22-R(n)\right]^{0.16}$
3238A/CF3052	0.05	$n=4.35\times10^{20}\left(s-193.85\right)^{-8.87}\left[283.69-R(n)\right]^{0.32}$
	10	$n=4.60\times10^{69}\left(s-29.98\right)^{-29.20}\left[237.81-R(n)\right]^{0.30}$

Table 7 Fatigue $s-n-R$ surface models of un-notched laminates.

Composites	Stress ratio	$s-n-R$ surface
3238A/EW250F	0.05	$n=9.75\times10^{17}\left(s-51.43\right)^{-7.28}\left[349.45-R(n)\right]^{0.59}$
	10	$n=1.13\times10^{21}\left(s-102.32\right)^{-8.79}\left[235.60-R(n)\right]^{0.16}$
3238A/CF3052	0.05	$n=4.35\times10^{20}\left(s-313.38\right)^{-8.87}\left[541.82-R(n)\right]^{0.32}$
	10	$n=4.60\times10^{69}\left(s-97.35\right)^{-29.20}\left[417.63-R(n)\right]^{0.30}$

Table 8 Comparison between the numerical predictions and the experimental results.

Composites	Block loading	Experi-ments	Palmgren–Miner rule	Relative Deviation %	Residual strength surface	Relative deviation %	Progressive damage analysis	Relative Deviation %

					model			
3238A /EW250F	H-L	228664	182901	20.01	196613	14.02	220925	3.38
	L-H	170820	182901	7.07	179465	5.06	181624	6.32
	H-L-H	158271	211738	33.78	132500	16.28	145710	7.94
3238A /CF3052	H-L-H	139276	199308	43.10	181500	30.32	113632	18.41

Notch effect on strength and fatigue life of woven composite laminates

Wan, Ao-Shuang

2019-06-15

Wan A, Xu Y, Xiong J. (2019) Notch effect on strength and fatigue life of woven composite laminates. International Journal of Fatigue, Volume 127, October 2019, pp. 275-290
https://doi.org/10.1016/j.ijfatigue.2019.06.017